Showcasing research from Professor Xiao's laboratory, School of Pharmaceutical Sciences, Wuhan University, Hubei, China.

Novel NIR-II organic fluorophores for bioimaging beyond 1550 nm

Highly twisted NIR-II small molecule fluorophores such as HL3 (45.5° at the S0 state) with the emission wavelength extending into 1550 nm were designed and synthesized using an aggregation induced emission (AIE) strategy. High-resolution in vivo imaging of the whole body, cerebral vasculature, and lymphatic drainage beyond 1550 nm was achieved using NIR-II AIE HL3 dots for the first time.

As featured in:

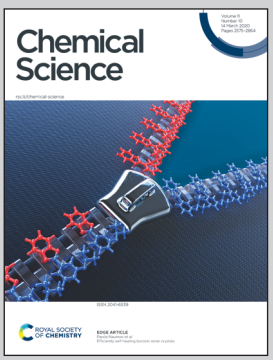

See Yuling Xiao *et al.*, *Chem. Sci.*, 2020, **11**, 2621.

ROYAL SOCIETY OF CHEMISTRY

rsc.li/chemical-science

Registered charity number: 207890

Chemical Science

ROYAL SOCIETY OF CHEMISTRY

EDGE ARTICLE

View Article Online
View Journal | View Issue

Cite this: *Chem. Sci.*, 2020, **11**, 2621

All publication charges for this article have been paid for by the Royal Society of Chemistry

Novel NIR-II organic fluorophores for bioimaging beyond 1550 nm†

Yang Li,‡[ab] Yufang Liu,‡[ab] Qianqian Li,[a] Xiaodong Zeng,[a] Tian Tian,[b] Wenyi Zhou,[a] Yan Cui,[b] Xikun Wang,[b] Xiaoding Cheng,[a] Qihang Ding,[a] Xiaofei Wang,[d] Junzhu Wu,[d] Hai Deng,[e] Yanqin Li,[a] Xianli Meng,[c] Zixin Deng,[a] Xuechuan Hong[ab] and Yuling Xiao *[a]

Received 30th December 2019
Accepted 5th February 2020

DOI: 10.1039/c9sc06567a

rsc.li/chemical-science

Near-infrared fluorescence imaging in the 1500–1700 nm sub-window (NIR-IIb) has shown a deeper penetration depth, higher resolution and zero auto-fluorescence for biomedical imaging. Till now, very few small molecule NIR-IIb fluorophores have been reported due to the extremely rare organic NIR-IIb skeleton and a notorious aggregation-caused quenching (ACQ) effect in aqueous solution. In this study, highly twisted NIR-II small molecule fluorophores such as **HL3** (45.5° at the S_0 state) with the emission wavelength extending into the NIR-IIb region were designed and synthesized using an aggregation-induced emission (AIE) strategy. **HL3** dots showed a remarkable increase in fluorescence intensity with a QY of 11.7% in the NIR-II window (>1000 nm) and 0.05% in the NIR-IIb region (>1550 nm) in water. High-resolution *in vivo* imaging of the whole body, cerebral vasculature, and lymphatic drainage beyond 1550 nm was achieved using NIR-II AIE **HL3** dots for the first time. These attractive results may promote the development of small-molecule NIR-IIb fluorophores with the maximum emission wavelength beyond 1500 nm with a deeper penetration depth and higher resolution.

Introduction

Optical fluorescence imaging is a promising modality for real-time monitoring of disease progression, drug delivery and image-guided surgery with high spatial and temporal resolution.[1] However, traditional fluorescence imaging techniques mostly focused on the visible and near-infrared region below 900 nm, where imaging resolution and penetration depths were largely limited due to the photo-scattering, auto-fluorescence and absorption of biological tissues. Hence, developing novel fluorophores with longer emission wavelengths to improve imaging resolution for *in vivo* deeper imaging is crucial and still a great challenge.[2]

During the past few years, molecular imaging in the second near-infrared region (NIR-II, 1000–1700 nm) has emerged as a powerful tool for the delineation and treatment of cancers.[3–12] The first organic small-molecule dye **CH1055** with 90% renal excretion for NIR-II bio-imaging was reported in 2015,[5] and opened up a new era for small molecule imaging. Deeper imaging depths (up to 3 cm), excellent temporal and spatial resolutions (50 FPS and 1 μm), and a higher tumor-to-normal tissue (T/NT) ratio (up to 15) were achieved in the NIR-II region.[5,12] Especially, the NIR-IIb sub-window (1500–1700 nm) showed tremendous advantages of near-zero auto-fluorescence, negligible scattering, and unparalleled tissue-imaging depths, and turned out to be a hot spot for *in vivo* fluorescence bio-imaging.[13] Very few inorganic NIR-IIb fluorophores such as single-walled carbon nanotubes (SWNTs), rare earth doped nanoparticles, and quantum dots have been investigated for biosensing and bioimaging beyond 1500 nm.[7g,8f,13–17] It is worth noting that organic **FD-1080** J-aggregates were first accomplished with high resolution imaging of the cerebral and hindlimb vasculature with fluorescence emission tailing into 1500 nm with a quantum yield (QY) of 0.0545%.[17] The signal-to-background ratio (SBR) was 3.3-fold higher than that of NIR-IIa (1300–1400 nm) imaging. However, small-molecule NIR-IIb fluorophores (beyond 1500 nm) are still in their infancy. Shifting small-molecule NIR-II fluorophore emissions, specifically into the NIR-IIb sub-window, is a great challenge but crucial for their expansion to *in vivo* biomedical applications. Thus, it is

[a]*State Key Laboratory of Virology, Key Laboratory of Combinatorial Biosynthesis and Drug Discovery (MOE), Hubei Province Engineering and Technology Research Center for Fluorinated Pharmaceuticals, Wuhan University School of Pharmaceutical Sciences, Wuhan 430071, China. E-mail: xiaoyl@whu.edu.cn*

[b]*College of Science, Innovation Center for Traditional Tibetan Medicine Modernization and Quality Control, Medical College, Tibet University, Lhasa, 850000, China*

[c]*Innovative Institute of Chinese Medicine and Pharmacy, Chengdu University of Traditional Chinese Medicine, Chengdu, Sichuan 611137, China*

[d]*Hubei Provincial Key Laboratory of Developmentally Originated Disease, Center for Experimental Basic Medical Education, Wuhan 430071, China*

[e]*Department of Chemistry, University of Aberdeen, Aberdeen, UK*

† Electronic supplementary information (ESI) available. See DOI: 10.1039/c9sc06567a

‡ These authors contributed equally to this work.

imperative to pursue new sorts of small molecule NIR-IIb dyes for enhanced optical imaging.

Here, we have rationally designed and synthesized new fluorescent probes **HL1–HL3** based on our previously reported NIR-II fluorophores **H1**[7d] and **Q4**.[6a] The hexyloxy chain substituted at positions R_1 and R_2 of thiophene not only served as a strong donor, but also significantly increased the dihedral angle up to 45.5° between BBTD and thiophene for the S_0 geometries (Fig. 1). Among them, **HL3** showed remarkable brightness, excellent AIE features with fluorescence emission stretching to 1550 nm and with a quantum yield of 0.05%. Furthermore, *in vivo* imaging beyond 1550 nm of the blood vessels, cerebral vasculature, and lymph nodes was achieved for the first time.

Results and discussion

A vast majority of small-molecule NIR-II contrast agents were synthesized using the donor–acceptor–donor (D–A–D) backbones, in which benzobisthiadiazole (BBTD) was used as the electron acceptor unit.[3–13] Nevertheless, the fluorescence quantum yields of organic NIR-II chromophores in aqueous solution were relatively low. The rigid planar aromatic structures with tremendous intermolecular π–π stacking interactions and the dominant non-radiative decay may be attributed to the aggregation-caused quenching (ACQ) effect in low-bandgap materials.[18] A feasible solution is to fully use the brightness of the dihedral twisted NIR-II backbones with strong emission extending into the NIR-IIb region by the aggregation-induced emission (AIE) strategy.[18–22] Thus, three novel organic small-molecule NIR-II fluorophores **HL1–HL3** were designed (Fig. 1). 3,4-bis(hexyloxy)thiophene served as the first donor (D1), and triphenylamine was utilized as the second donor (D2) and a building block of AIEgens. In addition, the influence of the electron-withdrawing group nitrobenzene and the electron donating group aminobenzene on the whole backbone was also investigated. Density functional theory (DFT) was first employed to calculate the electronic properties of **HL1–HL3** using Gaussian 09 software and the B3LYP/6-31G(d) method. For the optimized ground state (S_0) geometries, the twisted angles of **HL1–HL3**, **H1** and **Q4** were calculated. All dihedral angles of **HL1–HL3** between BBTD and donor 3,4-bis(hexyloxy)thiophene were ∼45° (Fig. 1), exhibiting more distortion than that of **Q4** (∼1.9°) and **H1** (∼0.3°) (Fig. S1†). The E_{gap} of **HL1** (1.78 eV) indicated short wavelength infrared characteristics (Table S1†). Moreover, the E_{gap} of **HL2** and **HL3** was 1.45 eV and 1.48 eV, respectively (Fig. S2†), lower than that of **CH1055** (1.5 eV) with a typical NIR-II optical E_{gap}, resulting in a hypsochromic shift compared to **H1** (1.21 eV) and **Q4** (1.12 eV) (Table S1†).

The small-molecule fluorophores **HL1–HL3** were synthesized mainly through Stille coupling, Zn reduction, *N*-thionylaniline-induced ring closure and Suzuki coupling in 45–50% yield over 4 steps from compound **1** (Fig. 2 and ESI†). The structures were confirmed by ^{1}H NMR, ^{13}C NMR, MALDI-TOF-MS or ESI-MS (Fig. S12–S26†). The spectroscopic properties of **HL1–HL3** in THF are shown in Fig. 3B and C, and it was found that their maximum emission wavelengths were ∼922 nm, 1062 nm and 1050 nm, respectively, which were consistent with the results of E_{gap} calculated using the Gaussian 09 software and 6-31G(d, p). **HL3** exhibited a remarkable increase in fluorescence intensity with a strong tail in the 1500 nm region (Fig. 3C). The molar extinction coefficients (ε) of **HL1–HL3** in THF were measured to be 8.3×10^3 L mol^{-1} cm^{-1}, 4.1×10^3 L mol^{-1} cm^{-1} and 7×10^3 L mol^{-1} cm^{-1}, respectively. The QYs of **HL1–HL3** in THF were measured to be 0.2%, 0.34% and 2% with IR-26 (QY: 0.5%) as a reference, respectively (Fig. S3†). The AIE properties of **HL1–HL3** were studied in the THF/water mixture solvents upon increasing the water volume fraction (f_w). As shown in Fig. 3A, **HL3** exhibited extremely strong fluorescence emission in THF/water with 90% f_w. To further confirm the AIE properties of **HL1–HL3**, the fluorescence emission spectra with different f_ws were subsequently obtained under 808 nm excitation (Fig. 3D, E and S4†). The fluorescence (FL) intensity of **HL1–HL3** gradually decreased with the increase of f_w from 0 to 40–50%, and increased sharply for **HL3** from f_w 50% to 90%, indicating a typical AIE characteristic. Meanwhile, no AIE characteristics were observed for **H1** and **Q4** under the similar conditions.

HL2 and **HL3** dots with high monodispersity and homogeneity were prepared in amphiphilic DPPE-5KPEG (Fig. 4A, S5 and S6†). **HL3** dots were characterized for bioimaging applications by transmission electron microscopy (TEM), dynamic light scattering (DLS) and the zeta potential with an average size of ∼90 nm, a dynamic size of ∼120 nm (Fig. 4B) and ∼ −9.2 eV, respectively (Fig. S7†). The encapsulation efficiency of **HL3** dots was calculated to be ∼82% (Fig. S8†). The maximum absorption wavelength was 750 nm (Fig. 4C). The maximum emission wavelength was centered at 1050 nm and tailed to 1600 nm

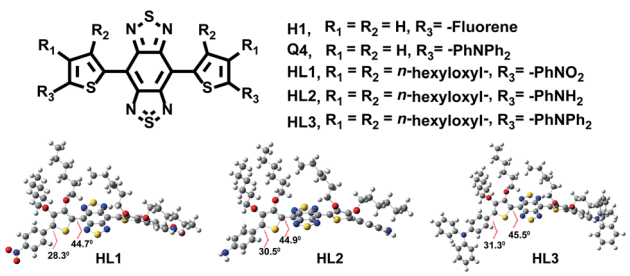

Fig. 1 The chemical structure and optimized ground state geometries (S_0) of **HL1–HL3** by using the Gaussian 09 software.

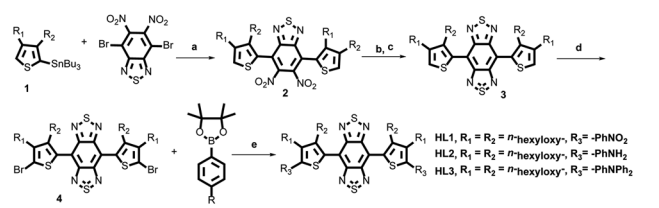

Fig. 2 The synthetic routes of **HL1–HL3**. Reagents and conditions: (a) $Pd(PPh_3)_4$ and THF; (b) Zn, NH_4Cl, and CH_2Cl_2/MeOH/H_2O; (c) PhNSO, TMSCl, and pyridine, two steps; (d) NBS, HBr, and DMF/CH_3CN; (e) $PdCl_2(dppf)_2CH_2Cl_2$ and K_2CO_3.

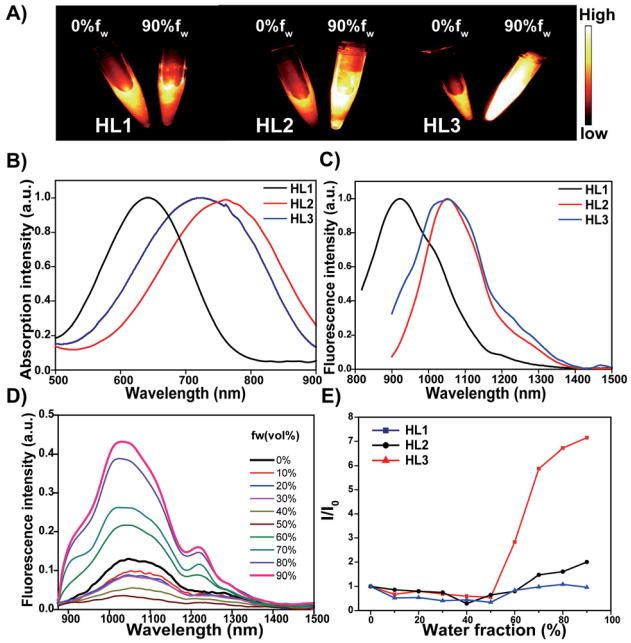

Fig. 3 (A) NIR-II fluorescence images (1000 LP, 808 nm excitation, 40 mW cm^{-2}, and 5 ms) of **HL1–HL3** in THF and THF/water (f_w 90%); (B) absorption and (C) fluorescence emission spectra of **HL1–HL3** in THF under 808 nm excitation; (D) fluorescence emission spectra of **HL3** obtained upon increasing f_w from 0 to 90% under 808 nm excitation; (E) fluorescence intensity ratios (I/I_0) of **HL1–HL3** in different f_ws, I_0 is the fluorescence intensity of **HL1–HL3** in THF.

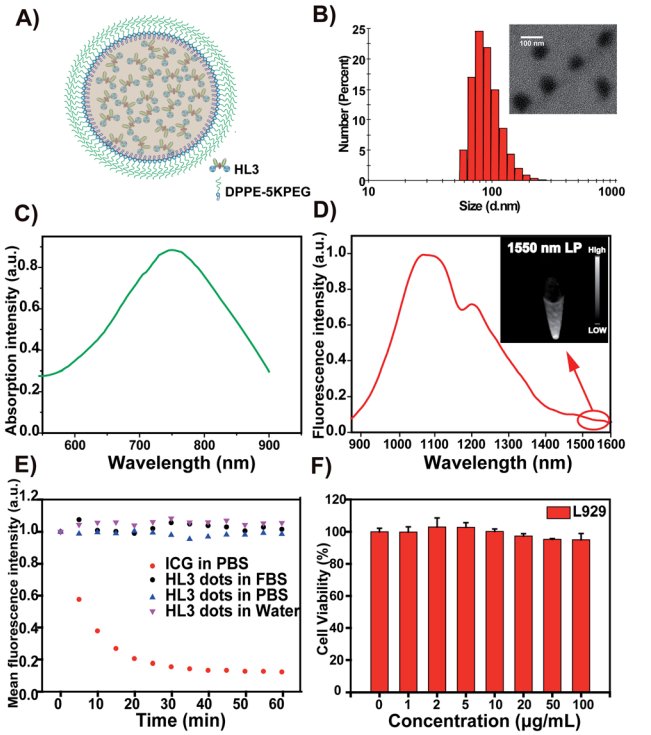

Fig. 4 (A) The formation of **HL3** dots *via* nanoprecipitation; (B) the DLS and TEM images of the **HL3** dots, scale bar: 100 nm; (C) the absorption spectra of **HL3** dots in water; (D) the fluorescence spectra of **HL3** dots, inset: NIR-IIb image of **HL3** dots (1550 nm LP, 808 nm excitation, 90 mW cm^{-2}, and 500 ms exposure time) at a concentration of 0.3 mg mL^{-1} in water; (E) the photo-stability of **HL3** dots in water, FBS, PBS and ICG in PBS with continuous 808 nm laser irradiation for 60 min (90 mW cm^{-2}); (F) the cytotoxicity of **HL3** dots.

(Fig. 4D). The quantum yields were calculated to be ~11.7% in the NIR-II region (1000–1700 nm) and ~0.05% in the NIR-IIb region (beyond 1550 nm). The molar extinction coefficient (ε) of **HL3** dots in water was measured to be 9.3×10^3 L mol^{-1} cm^{-1}. The reasonable quantum yields and NIR-IIb fluorescence emission of **HL3** dots encouraged us to explore their NIR-IIb imaging capabilities *in vitro*. **HL3** dots exhibited excellent fluorescence intensity beyond 1550 nm under 808 nm laser irradiation (1550 nm LP, Fig. 4D). As shown in Fig. 4E, the fluorescence intensity of the **HL3** dots showed no obvious changes in different media (FBS, PBS and water) under continuous 808 nm laser irradiation for 1 h (90 mW cm^{-2}). L929 mouse fibroblast cells were applied to evaluate the potential cytotoxicity of **HL3** dots using a standard 3-(4,5-dimethylthiazol-2-yl)-2,5-diphenyl tetrazolium bromide (MTT) assay. High cell viability was observed even at a high concentration (100 μg mL^{-1}, Fig. 4F). The pharmacokinetics of **HL3** dots were also investigated through the measurement of the blood circulation half-life. The blood half-life of **HL3** dots was 114 min (Fig. S9†). All these results have demonstrated that **HL3** dots have superior stability and excellent biocompatibility, and are more applicable for NIR-IIb bioimaging (beyond 1550 nm) *in vivo*.

To explore the feasibility of **HL3** dots as a novel AIE NIR-IIb probe for reliable imaging of the whole body and cerebral vasculature system in KM mice and C57BL/6 mice ($n = 3$ per group), **HL3** dots (200 μL, 1 mg mL^{-1}) were then injected into KM mice via the tail vein, and NIR-II and NIR-IIb images of blood vessels were recorded using an InGaAs camera with different LP filters (1000 nm, 1250 nm, and 1550 nm) and different exposure times under 808 nm laser irradiation (90 mW cm^{-2}). After 5 min post-injection, whole blood vessels were clearly visualized, and the hind limb vasculature was chosen for analysis *via* the Gaussian-fitted full width at half maximum (FWHM) (Fig. 5). It was found that the imaging of **HL3** dots in the NIR-II window (>1250 nm, 1250 nm LP) with a 50 ms exposure time exhibited highly superior resolution (Fig. 5B). An extended exposure time (500 ms) was needed for higher resolution NIR-IIb imaging beyond 1550 nm (>1550 nm, 1550 nm LP) (Fig. 5C). The FWHM values of the hind limb vasculature were 777 μm (1000 nm LP), 768 μm (1250 nm LP) and 719 μm (1550 nm LP), respectively. The signal-to-background ratio (SBR) of NIR-IIb imaging (SBR = 2.5, 1550 nm LP) was much higher than that of NIR-II imaging (SBR = 1.4, 1000 nm LP and SBR = 1.8, 1250 nm LP) (Fig. 5). The cerebral vasculature system was also imaged using the NIR-IIb probe **HL3** dots. The superior resolution of tiny vessels was obtained (Fig. 6). The corresponding SBR of NIR-II 1000 nm, NIR-II 1250 nm and NIR-IIb 1550 nm imaging was 1.4, 1.8 and 3.4, respectively (Fig. 6D and E). The SBR of NIR-IIb imaging (1550 nm LP) was 2.4-fold higher than that of NIR-II imaging (1000 nm LP). The FWHM values of the vessels at the same position (red dashed line) for different LP filters were calculated to be

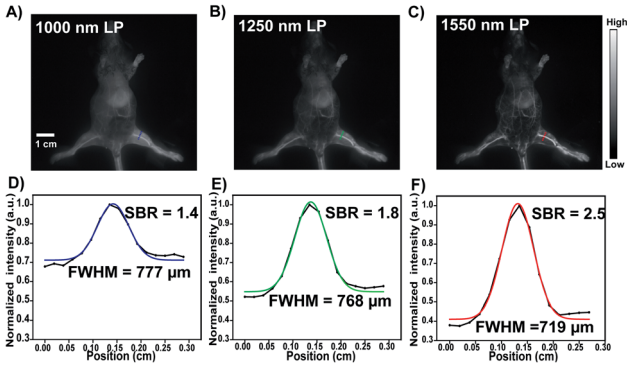

Fig. 5 NIR-II and NIR-IIb fluorescence images of whole mouse blood vessels after tail intravenous injection of **HL3** dots (200 μL, 1 mg mL^{-1}) under 808 nm laser excitation (90 mW cm^{-2}) with different long-pass filters (left to right: 1000 nm, 1250 nm and 1550 nm). Scale bar (A–C): 1 cm. (A) 1000 nm LP, 5 ms exposure time, and 90 mW cm^{-2}; (B) 1250 nm LP, 50 ms exposure time, and 90 mW cm^{-2}; (C) 1550 nm LP, 500 ms exposure time, and 90 mW cm^{-2}; (D–F) the fluorescence intensity profiles fitted using Gaussian, cross-section intensity (blue line), blue-dashed lines (1000 nm), green-dashed lines (1250 nm), red-dashed lines (1550 nm).

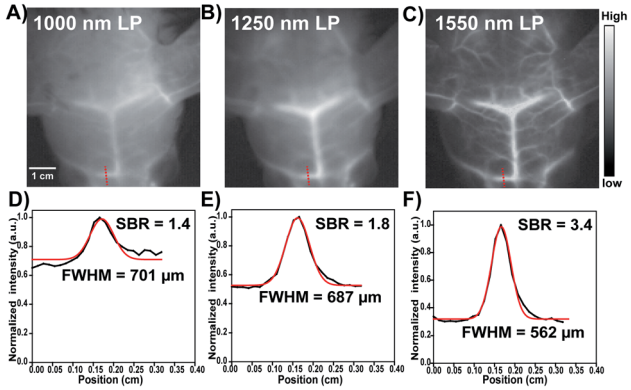

Fig. 6 NIR-II and NIR-IIb fluorescence images of cerebral vasculature with different LP filters in C57BL/6 mice (n = 3) after tail intravenous injection of **HL3** dots (200 μL, 1.5 mg mL^{-1}). Scale bars (A–C): 1 cm. (A) 1000 nm LP, 4 ms exposure time, and 90 mW cm^{-2}; (B) 1250 nm LP, 60 ms exposure time, and 90 mW cm^{-2}; (C) 1550 nm LP, 500 ms exposure time, and 90 mW cm^{-2}; (D–F) the fluorescence intensity profiles fitted using Gaussian, cross-section intensity (black lines), and the tiny vessel (red-dashed lines).

701 μm (1000 nm LP), 687 μm (1250 nm LP), and 562 μm (1550 nm LP), respectively. The NIR-II fluorescence images obtained using 1000 nm, 1250 nm and 1550 nm LP were also evaluated at the same exposure time (200 ms) at a concentration of 0.8 mg mL^{-1}. It was found that **HL3** saturated the detector with 1000 nm and 1250 nm long-pass filters under imaging conditions suitable for **HL3** with a 1550 nm long-pass filter (Fig. S10†). All these results indicated that **HL3** dots have great potential for *in vivo* NIR-IIb imaging (beyond 1500 nm) at an extended exposure time.

The lymph node drainage plays a vital role in tumor metastasis. We next demonstrated the application of **HL3** dots for

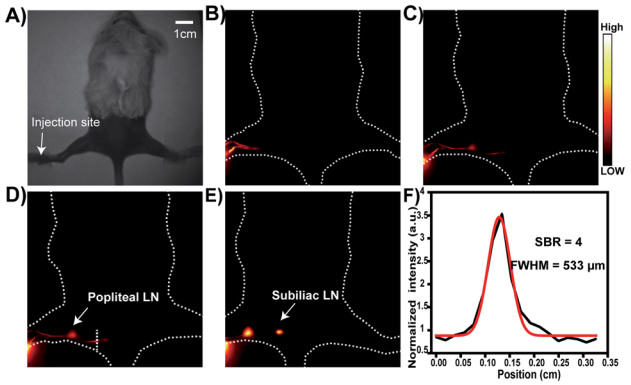

Fig. 7 Dynamic NIR-IIb imaging of lymphatic drainage in KM normal mice (n = 3) after injection of **HL3** dots (15 μL, 1 mg mL^{-1}) under 808 nm laser excitation (1550 nm LP, 500 ms, and 90 mW cm^{-2}). (A) The digital photograph and *in vivo* NIR-II fluorescence imaging at 0 min; (B) 1 min; (C) 30 min; (D) 1 h; (E) 3 h after injection. (F) The fluorescence intensity profiles fitted using Gaussian in (D), cross-section intensity (black line) and the lymphatic vessel (white-dashed lines).

lymph node NIR-IIb imaging (beyond 1550 nm). **HL3** dots (15 μL, 1 mg mL^{-1}) were injected intra-dermally at the left forefoot pad of KM mice (n = 3 per group) (Fig. 7). The process of lymphatic drainage was monitored under 808 nm laser irradiation (90 mW cm^{-2}) using 1550 nm LP. Lymphatic vessels were notably identified in 1 min after injection. The popliteal lymph node was gradually lighted up, and both the popliteal lymph node and the subiliac lymph node were clearly visualized in 2 h. The diameter of the lymphatic vessel between the popliteal lymph node and the subiliac lymph node was calculated to be 533 μm *via* FWHM, and the SBR reached 4 (Fig. 7F). The SBR values of the popliteal lymph node and the subiliac lymph node were 2.5 and 3.2 (1000 nm LP), 2.9 and 3.4 (1250 nm LP), and 5.1 and 4.8 (1550 nm LP), respectively (Fig. S11†). These results reveal that NIR-IIb imaging beyond 1550 nm of lymph node drainage can be achieved with a higher SBR.

Experimental section

All animal experiments were performed according to the Chinese Regulations for the Administration of Affairs Concerning Experimental Animals and approved by the Institutional Animal Care and Use Committee (IACUC) of Wuhan University. And all the experimental details are provided in the ESI.†

Conclusions

In summary, we have successfully synthesized a series of small molecule fluorophores **HL1–HL3** by introducing different donors and distortion groups. Among them, **HL3** showed extremely stronger AIE characteristics and highly twisted donor–acceptor distortion. **HL3** dots exhibited excellent water solubility, photo-stability and biocompatibility with a remarkable increase in NIR-II fluorescence intensity with QYs of 11.7%

and 0.05% in the NIR-II (>1000 nm) and NIR-IIb region (>1550 nm), respectively, in water. Superior quality NIR-IIb imaging beyond 1550 nm of the whole body, cerebral vasculature and the lymphatic drainage system was demonstrated for the first time with a higher SBR. It is hoped that this novel NIR-II fluorophore **HL3** obtained using an integrated AIE and D–A distortion strategy may become a practical strategy to develop small-molecule NIR-IIb fluorophores with the maximum emission wavelength beyond 1500 nm with a deeper penetration depth and higher resolution.

Conflicts of interest

There are no conflicts to declare.

Acknowledgements

This work was partially supported by grants from NSFC (81773674, 81573383, and 21473041), NSFHP (2017CFA024, 2017CFB711, and 2016ACA126), the Applied Basic Research Program of WMBST (2019020701011429), Tibet Autonomous Region Science and Technology Plan Project Key Project (XZ201901-GB-11), Project First-Class Disciplines Development Supported by Chengdu University of Traditional Chinese Medicine (CZYJC1903), and Health Commission of Hubei Province Scientific Research Project (WJ2019M177 and WJ2019M178).

Notes and references

1 G. Hong, A. L. Antaris and H. Dai, *Nat. Biomed. Eng.*, 2017, **1**, 0010.

2 S. He, J. Song, J. Qu and Z. Cheng, *Chem. Soc. Rev.*, 2018, **47**, 4258–4278.

3 (*a*) G. Hong, J. C. Lee, J. T. Robinson, U. Raaz, L. Xie, N. F. Huang, J. P. Cooke and H. Dai, *Nat. Med.*, 2012, **18**, 1841; (*b*) Y. Du, B. Xu, T. Fu, M. Cai, F. Li, Y. Zhang and Q. Wang, *J. Am. Chem. Soc.*, 2010, **132**, 1470–1471; (*c*) G. Hong, J. T. Robinson, Y. Zhang, S. Diao, A. L. Antaris, Q. Wang and H. Dai, *Angew. Chem., Int. Ed.*, 2012, **51**, 9818–9821; (*d*) Y. Sun, X. Ma, K. Cheng, B. Wu, J. Duan, H. Chen, L. Bu, R. Zhang, X. Hu, Z. Deng, L. Xing, X. Hong and Z. Cheng, *Angew. Chem., Int. Ed.*, 2015, **54**, 5981–5984.

4 (*a*) G. Chen, F. Tian, C. Li, Y. Zhang, Z. Weng, Y. Zhang, R. Peng and Q. Wang, *Biomaterials*, 2015, **53**, 265–273; (*b*) G. Hong, S. Diao, J. Chang, A. L. Antaris, C. Chen, Z. Bo, Z. Su, D. N. Atochin, P. L. Huang, K. I. Andreasson, C. J. Kuo and H. Dai, *Nat. Photonics*, 2014, **8**, 723–730; (*c*) S. Diao, J. L. Blackburn, G. Hong, A. L. Antaris, J. Chang, J. Z. Wu, B. Zhang, K. Cheng, C. J. Kuo and H. Dai, *Angew. Chem., Int. Ed.*, 2015, **54**(49), 14758–14762; (*d*) R. Wang, X. Li, L. Zhou and F. Zhang, *Angew. Chem., Int. Ed.*, 2014, **53**, 12086–12090; (*e*) D. Naczynski, M. Tan, M. Zevon, B. Wall, J. Kohl, A. Kulesa, S. Chen, C. Roth, R. Riman and P. Moghe, *Nat. Commun.*, 2013, **4**, 2199; (*f*) J. Lin, Q. Li, X. Zeng, Z. Chen, Q. Ding, Y. Li, H. Zhou, X. Meng, D. Chen, Z. Deng, X. Hong and Y. Xiao, *Sci. China: Chem.*, 2020, DOI: 10.1007/s11426-019-9685-6.

5 (*a*) A. L. Antaris, H. Chen, K. Cheng, Y. Sun, G. Hong, C. Qu, S. Diao, Z. Deng, X. Hu, B. Zhang, X. Zhang, O. K. Yaghi, Z. R. Alamparambil, X. Hong, Z. Cheng and H. Dai, *Nat. Mater.*, 2016, **15**, 235–242; (*b*) A. L. Antaris, H. Chen, S. Diao, Z. Ma, Z. Zhang, S. Zhu, J. Wang, A. X. Lozano, Q. Fan, L. Chew, M. Zhu, K. Cheng, X. Hong, H. Dai and Z. Cheng, *Nat. Commun.*, 2017, **8**, 15269.

6 (*a*) Y. Sun, C. Qu, H. Chen, M. He, C. Tang, K. Shou, S. Hong, M. Yang, Y. Jiang, B. Ding, Y. Xiao, L. Xing, X. Hong and Z. Cheng, *Chem. Sci.*, 2016, **7**, 6203–6207; (*b*) J.-Y. Zhao, G. Chen, Y.-P. Gu, R. Cui, Z.-L. Zhang, Z.-L. Yu, B. Tang, Y.-F. Zhao and D.-W. Pang, *J. Am. Chem. Soc.*, 2016, **138**, 1893–1903; (*c*) X. D. Zhang, H. Wang, A. L. Antaris, L. Li, S. Diao, R. Ma, A. Nguyen, G. Hong, Z. Ma, J. Wang, S. Zhu, J. M. Castellano, T. Coray, Y. Liang, J. Luo and H. Dai, *Adv. Mater.*, 2016, **28**, 6872; (*d*) X. Dang, L. Gu, J. Qi, S. Correa, G. Zhang, A. M. Belcher and P. T. Hammond, *Proc. Natl. Acad. Sci. U. S. A.*, 2016, **113**, 5179–5184.

7 (*a*) Z. Lei, X. Li, X. Luo, H. He, J. Zheng, X. Qian and Y. Yang, *Angew. Chem., Int. Ed.*, 2017, **56**, 2979–2983; (*b*) E. D. Cosco, J. R. Caram, O. T. Bruns, D. Franke, R. A. Day, E. P. Farr, M. G. Bawendi and E. M. Sletten, *Angew. Chem., Int. Ed.*, 2017, **56**, 13126–13129; (*c*) S. Zhu, Q. Yang, A. L. Antaris, J. Yue, Z. Ma, H. Wang, W. Huang, H. Wan, J. Wang, S. Diao, B. Zhang, X. Li, Y. Zhong, K. Yu, G. Hong, J. Luo, Y. Liang and H. Dai, *Proc. Natl. Acad. Sci. U. S. A.*, 2017, **114**, 962–967; (*d*) Y. Sun, M. Ding, X. Zeng, Y. Xiao, H. Wu, H. Zhou, B. Ding, C. Qu, W. Hou, A. Er-bu, Y. Zhang, Z. Cheng and X. Hong, *Chem. Sci.*, 2017, **8**, 3489–3493; (*e*) Y. Feng, S. Zhu, A. L. Antaris, H. Chen, Y. Xiao, X. Lu, L. Jiang, S. Diao, K. Yu and Y. Wang, *Chem. Sci.*, 2017, **8**, 3703–3711; (*f*) C. Li, Y. Zhang, G. Chen, F. Hu, K. Zhao and Q. Wang, *Adv. Mater.*, 2017, **29**, 1605754; (*g*) Y. Zhong, Z. Ma, S. Zhu, J. Yue, M. Zhang, A. L. Antaris, J. Yuan, R. Cui, H. Wan, Y. Zhou, W. Wang, N. F. Huang, J. Luo, Z. Hu and H. Dai, *Nat. Commun.*, 2017, **8**, 737; (*h*) Y. Feng, S. Zhu, A. L. Antaris, H. Chen, Y. Xiao, X. Lu, L. Jiang, S. Diao, K. Yu, Y. Wang, S. Herraiz, J. Yue, X. Hong, G. Hong, Z. Cheng, H. Dai and A. J. Hsueh, *Chem. Sci.*, 2017, **8**, 3703–3711.

8 (*a*) J. A. Carr, D. Franke, J. R. Caram, C. F. Perkinson, M. Saif, V. Askoxylakis, M. Datta, D. Fukumura, R. K. Jain, M. G. Bawendi and O. T. Bruns, *Proc. Natl. Acad. Sci. U. S. A.*, 2018, **115**, 4465–4470; (*b*) Y. Sun, X. Zeng, Y. Xiao, C. Liu, H. Zhu, H. Zhou, Z. Chen, F. Xu, M. Zhu, J. Wu, H. Zhang, Z. Deng, Z. Cheng and X. Hong, *Chem. Sci.*, 2018, **9**, 2092–2097; (*c*) B. Li, L. Lu, M. Zhao, Z. Lei and F. Zhang, *Angew. Chem., Int. Ed.*, 2018, **57**, 1–6; (*d*) H. Wan, J. Yue, S. Zhu, T. Uno, X. Zhang, Q. Yang, K. Yu, G. Hong, J. Wang, L. Li, Z. Ma, H. Gao, Y. Zhong, J. Su, A. L. Antaris, Y. Xia, J. Luo, Y. Liang and H. Dai, *Nat. Commun.*, 2018, **9**, 1171; (*e*) Z. Sheng, B. Guo, D. Hu, S. Xu, W. Wu, W. H. Liew, K. Yao, J. Jiang, C. Liu, H. Zheng and B. Liu, *Adv. Mater.*, 2018, **30**, 1800766; (*f*) Y. Fan, P. Wang, Y. Lu,

R. Wang, L. Zhou, X. Zheng, X. Li, J. A. Piper and F. Zhang, *Nat. Nanotechnol.*, 2018, **13**, 941; (*g*) S. Zhu, S. Herraiz, J. Yue, M. Zhang, H. Wan, Q. Yang, Z. Ma, Y. Wang, J. He, A. L. Antaris, Y. Zhong, S. Diao, Y. Feng, Y. Zhou, K. Yu, G. Hong, Y. Liang, A. J. Hsueh and H. Dai, *Adv. Mater.*, 2018, **30**, 1705799; (*h*) Z. Xue, S. Zeng and J. Hao, *Biomaterials*, 2018, **171**, 153–163; (*i*) Z. Ma, M. Zhang, J. Yue, C. Alcazar, Y. Zhong, T. C. Doyle, H. Dai and N. F. Huang, *Adv. Funct. Mater.*, 2018, **28**, 1803417; (*j*) M. Zhang, J. Yue, R. Cui, Z. Ma, H. Wan, F. Wang, S. Zhu, Y. Zhou, Y. Kuang, Y. Zhong, D.-W. Pang and H. Dai, *Proc. Natl. Acad. Sci. U. S. A.*, 2018, **115**(26), 6590; (*k*) X. Lei, R. Li, D. Tu, X. Shang, Y. Liu, W. You, C. Sun, F. Zhang and X. Chen, *Chem. Sci.*, 2018, **9**, 4682.

9 (*a*) X. Zeng, Y. Xiao and X. Hong, *Adv. Healthcare Mater.*, 2018, **7**, 1800589; (*b*) Y. Xu, M. Tian, H. Zhang, Y. Xiao, X. Hong and Y. Sun, *Chin. Chem. Lett.*, 2018, **29**, 1093–1097; (*c*) W. Zhu, *Sci. China: Chem.*, 2016, **59**, 203–204; (*d*) H. Zhou, Y. Xiao and X. Hong, *Chin. Chem. Lett.*, 2018, **29**, 1425–1428; (*e*) J. Yang and X. Hong, *Sci. China: Chem.*, 2019, **62**, 7–8.

10 (*a*) R. Tian, H. Ma, Q. Yang, H. Wan, S. Zhu, S. Chandra, H. Sun, D. Kiesewetter, G. Niu, Y. Liang and X. Chen, *Chem. Sci.*, 2019, **10**, 326; (*b*) C. Qu, Y. Xiao, H. Zhou, J. Lin, X. Zeng, H. Chen, K. Qian, X. Zhang, J. Wu, Z. Deng, Z. Cheng and X. Hong, *Adv. Opt. Mater.*, 2019, **7**, 1900229; (*c*) Z. Hu, C. Fang, B. Li, Z. Zhang, C. Cao, M. Cai, S. Su, X. Sun, X. Shi, C. Li, T. Zhou, Y. Zhang, C. Chi, P. He, X. Xia, Y. Chen, S. S. Gambhir, Z. Cheng and J. Tian, *Nat. Biomed. Eng.*, 2019, DOI: 10.1038/s41551-019-0494-0; (*d*) B. Ding, Y. Xiao, H. Zhou, X. Zhang, C. Qu, F. Xu, Z. Deng, Z. Cheng and X. Hong, *J. Med. Chem.*, 2019, **62**, 2049–2059; (*e*) X. Zeng, Z. Chen, L. Tang, H. Yang, N. Liu, H. Zhou, Z. Deng, Y. Yu, H. Deng, X. Hong and Y. Xiao, *Chem. Commun.*, 2019, **55**, 2541–2544; (*f*) F. Wang, H. Wan, Z. Ma, Y. Zhong, Q. Sun, Y. Tian, L. Qu, H. Du, M. Zhang, L. Li, H. Ma, J. Luo, Y. Liang, W. Li, G. Hong, L. Liu and H. Dai, *Nat. Methods*, 2019, **16**, 545–552; (*g*) S. Zhu, R. Tian, A. L. Antaris, X. Chen and H. Dai, *Adv. Mater.*, 2019, **31**, 1900321; (*h*) J. Huang, C. Xie, X. Zhang, Y. Jiang, J. Li, Q. Fan and K. Pu, *Angew. Chem., Int. Ed.*, 2019, **58**, 15120–15127; (*i*) Y. Sun, F. Ding, Z. Zhou, C. Li, M. Pu, H. Li, G. Yang, Y. Sun and P. J. Stang, *Proc. Natl. Acad. Sci. U. S. A.*, 2019, **116**, 1968–1973; (*j*) Q. Wang, Y. Dai, J. Xu, J. Cai, X. Niu, L. Zhang, R. Chen, Q. Shen, W. Huang and Q. Fan, *Adv. Funct. Mater.*, 2019, **29**, 1901480; (*k*) B. Guo, Z. Feng, D. Hu, S. Xu, E. Middha, Y. Pan, C. Liu, H. Zheng, J. Qian, Z. Sheng and B. Liu, *Adv. Mater.*, 2019, **13**, 1902504; (*l*) Z. Zhang, X. Fang, Z. Liu, H. Liu, D. Chen, S. He, J. Zheng, B. Yang, W. Qin, X. Zhang and C. Wu, *Angew. Chem., Int. Ed.*, 2019, DOI: 10.1002/anie.201914397; (*m*) R. Tian, Q. Zeng, S. Zhu, J. Lau, S. Chandra, R. Ertsey, K. Hettie, T. Teraphongphom, Z. Hu, G. Niu, D. Kiesewetter, H. Sun, X. Zhang, A. Antaris, B. Brooks and X. Chen, *Sci. Adv.*, 2019, **5**, eaaw0672J.

11 Y. Chen, D. M. Montana, H. Wei, J. M. Cordero, M. Schneider, X. L. Guével, O. Chen, O. T. Bruns and M. G. Bawendi, *Nano Lett.*, 2017, **17**, 6330–6334.

12 Y. Cai, Z. Wei, C. Song, C. Tang, W. Han and X. Dong, *Chem. Soc. Rev.*, 2019, **48**, 22–37.

13 S. Diao, J. L. Blackburn, G. Hong, A. L. Antaris, J. Chang, J. Z. Wu, B. Zhang, K. Cheng, C. J. Kuo and H. Dai, *Angew. Chem., Int. Ed.*, 2015, **54**, 1–6.

14 Z. Deng, X. Li, Z. Xue, M. Jiang, Y. Li, S. Zeng and H. Liu, *Nanoscale*, 2018, **10**, 9393–9400.

15 Y. Li, S. Zeng and J. Hao, *ACS Nano*, 2019, **13**, 248–259.

16 S. Wang, L. Liu, Y. Fan, A. M. El-Toni, M. S. Alhoshan, D. Li and F. Zhang, *Nano Lett.*, 2019, **19**, 2418–2427.

17 C. Sun, B. Li, M. Zhao, S. Wang, Z. Lei, L. Lu, H. Zhang, L. Feng, C. Dou, D. Yin, H. Xu, Y. Cheng and F. Zhang, *J. Am. Chem. Soc.*, 2019, **141**, 19221–19225.

18 (*a*) J. Mei, N. L. C. Leung, R. T. K. Kwok, J. W. Y. Lam and B. Z. Tang, *Chem. Rev.*, 2015, **115**, 11718–11940; (*b*) J. Qi, C. Sun, D. Li, H. Zhang, W. Yu, A. Zebibula, J. W. Y. Lam, W. Xi, L. Zhu, F. Cai, P. Wei, C. Zhu, R. T. K. Kwok, L. L. Streich, R. Prevedel, J. Qian and B. Z. Tang, *ACS Nano*, 2018, **12**, 7936–7945.

19 (*a*) J. Liu, C. Chen, S. Ji, Q. Liu, D. Ding, D. Zhao and B. Liu, *Chem. Sci.*, 2017, **8**, 2782–2789; (*b*) W. Wu, Y. Yang, Y. Yang, Y. Yang, K. Zhang, L. Guo, H. Ge, X. Chen, J. Liu and H. Feng, *Small*, 2019, **15**, 1805549; (*c*) S. Wang, J. Liu, C. C. Goh, L. G. Ng and B. Liu, *Adv. Mater.*, 2019, **31**, 1904447; (*d*) W. Wu, Y.-Q. Yang, Y. Yang, Y.-M. Yang, H. Wang, K.-Y. Zhang, L. Guo, H.-F. Ge, J. Liu and H. Feng, *Int. J. Nanomed.*, 2019, **14**, 3571.

20 Q. Yang, Z. Hu, S. Zhu, R. Ma, H. Ma, Z. Ma, H. Wan, T. Zhu, Z. Jiang, W. Liu, L. Jiao, H. Sun, Y. Liang and H. Dai, *J. Am. Chem. Soc.*, 2018, **140**, 1715–1724.

21 J. Lin, X. Zeng, Y. Xiao, L. Tang, J. Nong, Y. Liu, H. Zhou, B. Ding, F. Xu, H. Tong, Z. Deng and X. Hong, *Chem. Sci.*, 2019, **10**, 1219–1226.

22 S. Liu, X. Zhou, H. Zhang, H. Ou, J. W. Y. Lam, Y. Liu, L. Shi, D. Ding and B. Z. Tang, *J. Am. Chem. Soc.*, 2019, **141**, 5359–5368.